Department of Mechanical & Electro-Mechanical Engineering
National Sun Yat-Sen University
Kaohsiung, Taiwan 80424, China

Pore Formation in Solid during Manufacturing and Materials Processing

P. S. Wei *
Distinguished Research Professor
FASME, FAWS

* E-mail: pswei@mail.nsysu.edu.tw

Dept. Mechanical & Electro-Mechanical Eng., NSYSU
Kaohsiung, Taiwan, China

Abstract

- Mechanisms of pore formation in solid during materials processing and manufacturing are studied from experimental observations and quantitative interpretations of behavior of a bubble trapped in solid during solidification in this note. Formation of bubbles is resulted from supersaturation of the dissolved gas in the liquid ahead of the solidification front. The pores in solids are widely encountered in micro-electro-mechanical systems (MEMS), manufacturing, materials and bioscience fields. To facilitate analysis, the development of the bubble or pore in solid can be classified into five regimes: (1) nucleation on the solidification front, (2) spherical growth of the bubble, (3) solidification rate-controlled elongation, (4) disappearance of the bubble in the solid, and (5) formation of the pores. Owing to quite different and irregular pore shapes, systematical investigations of complicated bubble dynamics in the solid during freezing are becoming important and challenging issues. Some of analyses, models and future topics are presented in this work.

Dept. Mechanical & Electro-Mechanical Eng., NSYSU
Kaohsiung, Taiwan, China

Content

- Introduction
- Experimental setup and measurements
- Bubble formation
- Model for bubble entrapment
- Solution procedure chart
- Governing equations and boundary conditions
- Simplified models
- Wormhole formation
- Future topics
- Examples
- Conclusions

Dept. Mechanical & Electro-Mechanical Eng., NSYSU
Kaohsiung, Taiwan, China

Introduction

- Chalmers (1959): Wormholes due to air supersaturation in water at solidification front are observed and interpreted from solute diffusion viewpoint.
- Grigorenko (1970): Pores in welds occur for supersaturation ratio at S-L interface greater than unity.
- Wilcox and Kuo (1973): Bubble nucleation and growth ahead of solidification front of multicomponent solutions are interpreted from momentum balance, solute transport, segregation and physico-chemical theories.
- Vasconcellos and Beech (1975): Blowhole shapes are observed and explained from solute profile in ice/water/carbon dioxide system.
- Geguzin and Dzyuba (1977): The bubbles observed arise chiefly in the region of coarse distortion of solidification front. Volume density and mean size of pores in ice as functions of solidification rate are measured

Continued

- Geguzin and Dzuba (1981): Periodic formation of pores due to alternative accumulation and drop down of solute concentration are observed by using the test bubble method. A bubble may not be captured or captured as an elongated pore, or isolated pore, depending on relative speed between the bubble cap and solidification rate.
- Wei et al. (2000): A spherical cap-shaped bubble with a specified contact angle is proposed to predict pore shapes in solid by accounting for mass, momentum and energy transport and physico-chemical theories. The analysis is extended by Wei and Ho (2001) to determine self-consistent contact angles.
- Murakami and Nakajima (2002): Spherical, columnar and periodic pores, and interfacial morphology as function of saturation, pressure, and solidification rate are observed and measured.
- Wei et al. (2004): In situ measurements of bubble and pore shapes are conducted. Five stages of pore formation are proposed and modeled.

Dept. Mechanical & Electro-Mechanical Eng., NSYSU
Kaohsiung, Taiwan, China

Experimental Setup and Measurements (Wei et al. 2003,2004)

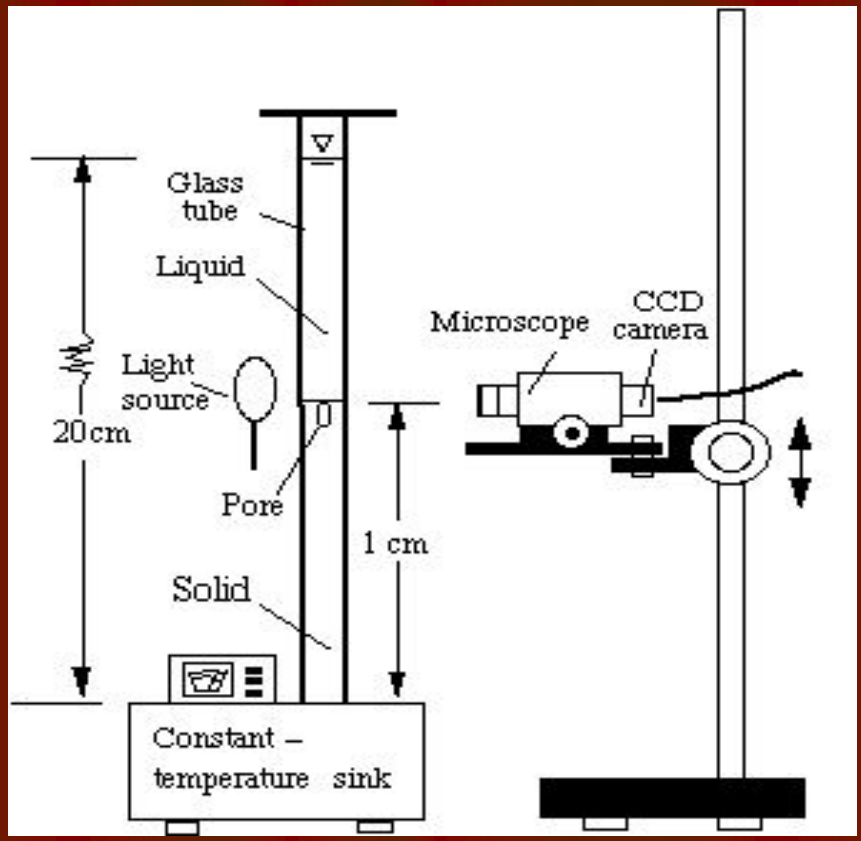

Dept. Mechanical & Electro-Mechanical Eng., NSYSU
Kaohsiung, Taiwan, China

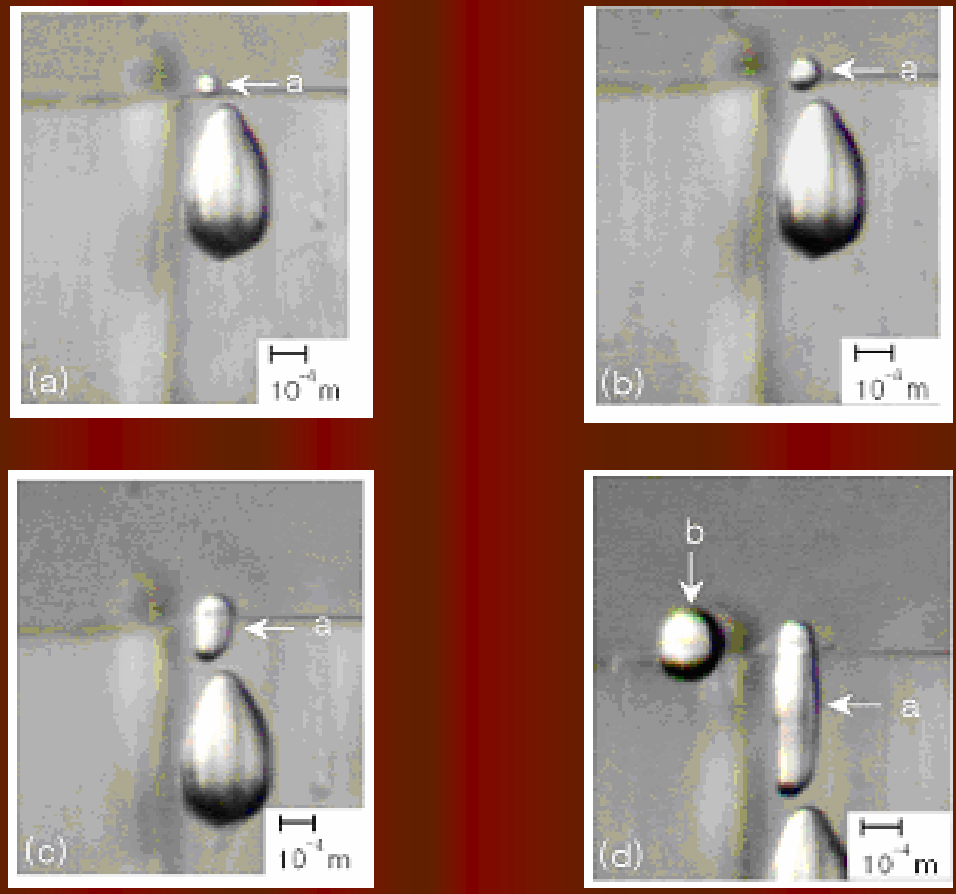

Dept. Mechanical & Electro-Mechanical Eng., NSYSU
Kaohsiung, Taiwan, China

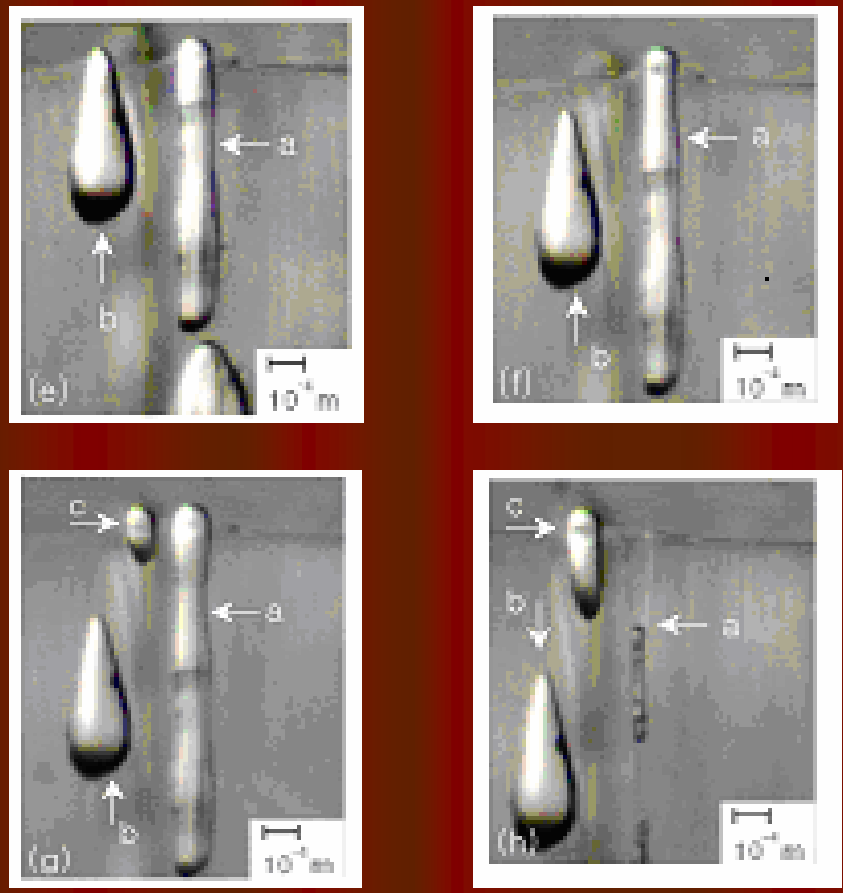

Bubbles trapped in solid at different times or locations near the location of 1 cm (a) 0, (b) 5, (c) 20, (d) 60, (e) 120, (f) 150, (g) 180, and (h) 206 s during the freezing of water containing oxygen gas content of 0.0041 g/100 g and temperature of the constant temperature sink of -25^{0}C.

Dept. Mechanical & Electro-Mechanical Eng., NSYSU
Kaohsiung, Taiwan, China

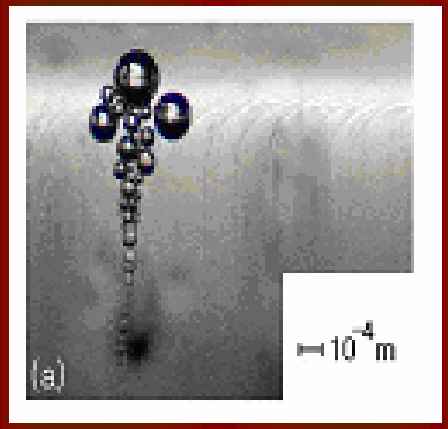

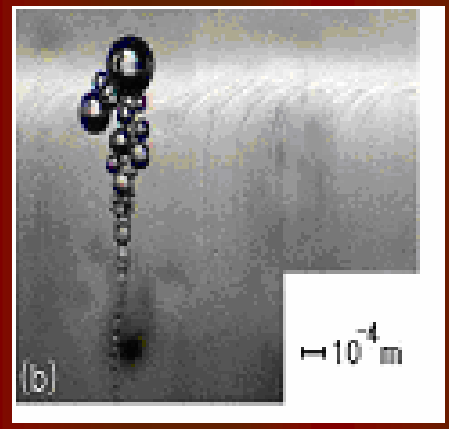

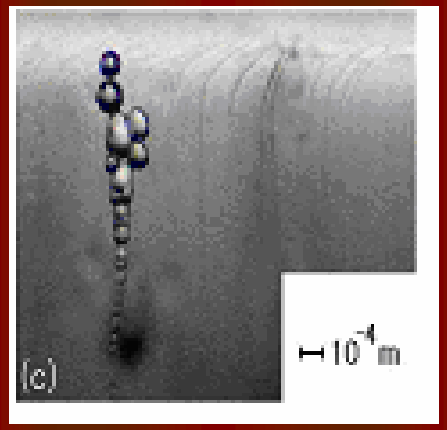

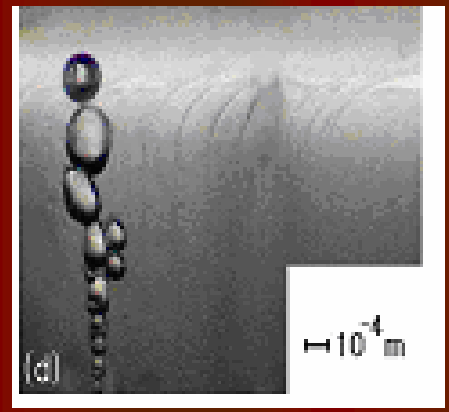

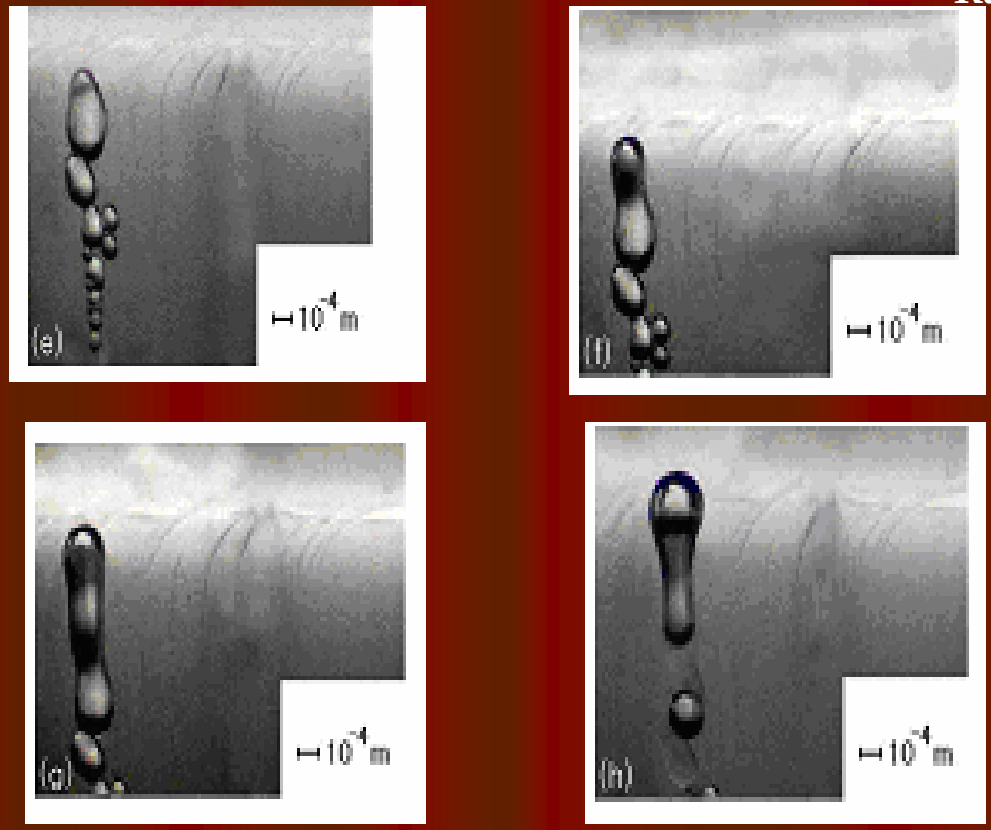

Bubbles trapped in solid at different times or locations near a location of 1 cm (a) 0 s, (b) 450 s, (c) 540 s, (d) 810 s, (e) 900 s, (f) 1170 s, (9) 1350 s, (h) 1440 s during the freezing of water containing oxygen gas content of 0.0037 g/100 g and temperature of -25^0C of the constant temperature sink.

Dept. Mechanical & Electro-Mechanical Eng., NSYSU
Kaohsiung, Taiwan, China

Temperature-Time Diagrams for Different Cooling Temperatures

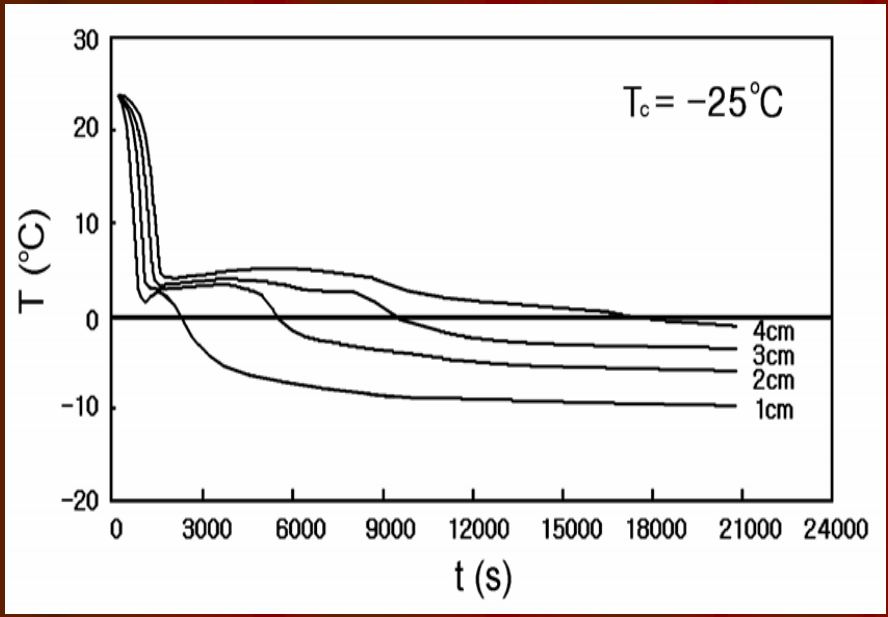

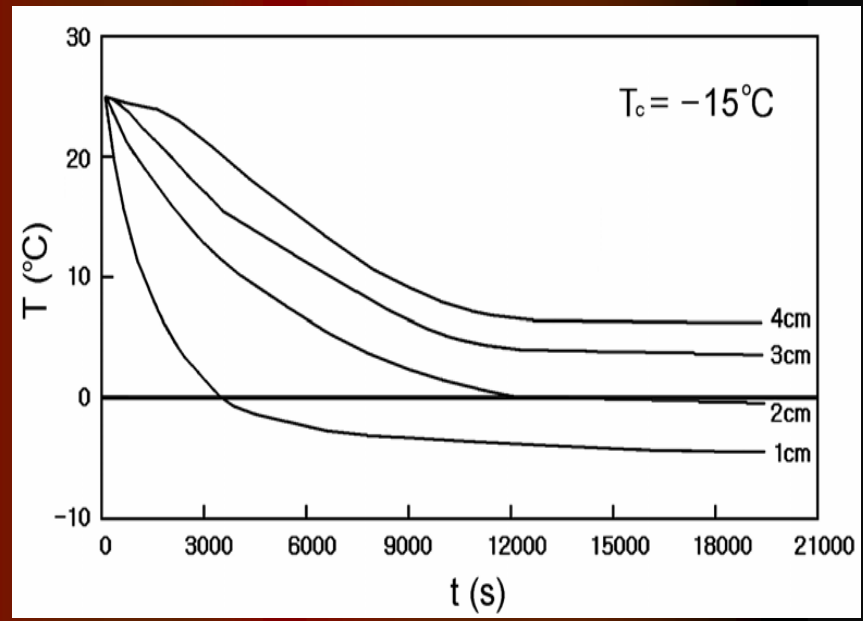

Dept. Mechanical & Electro-Mechanical Eng., NSYSU
Kaohsiung, Taiwan, China

Solidification Front Location –Time Diagram

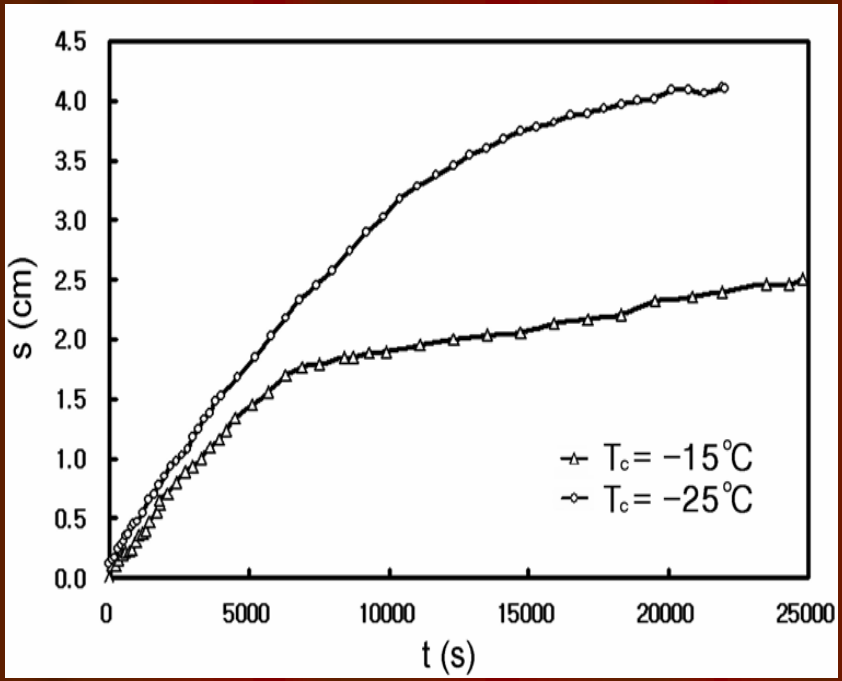

Concentration Profile – Time Diagram

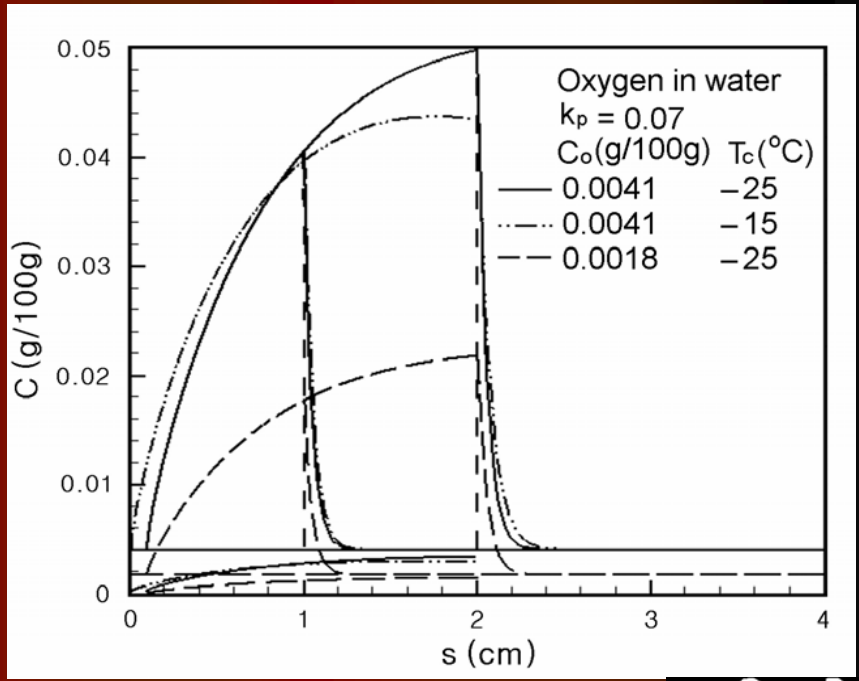

Dept. Mechanical & Electro-Mechanical Eng., NSYSU
Kaohsiung, Taiwan, China

In Situ Measurement of Pore Shapes

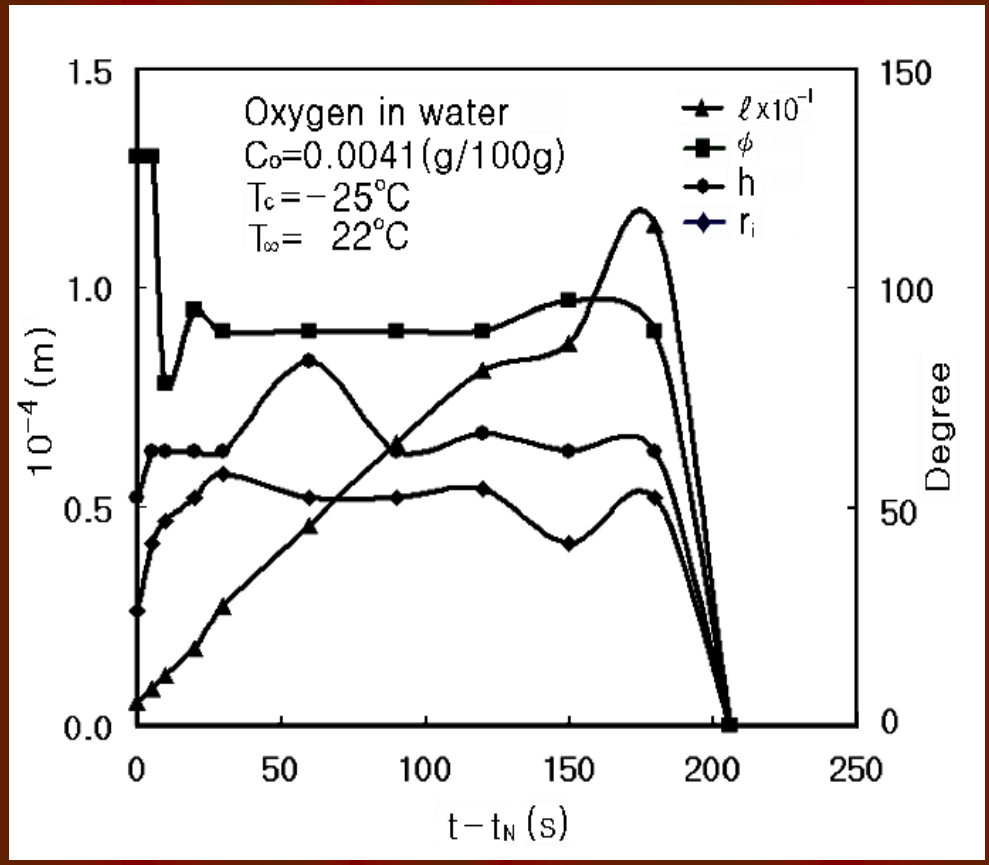

Suggested Stages for Pore Formation (Wei et al. 2004)

- Nucleation on solidification front
- Spherical growth
- Solidification rate-controlled elongation
- Disappearance of the bubble
- Pore formation in solid

Dept. Mechanical & Electro-Mechanical Eng., NSYSU
Kaohsiung, Taiwan, China

Bubble Formation

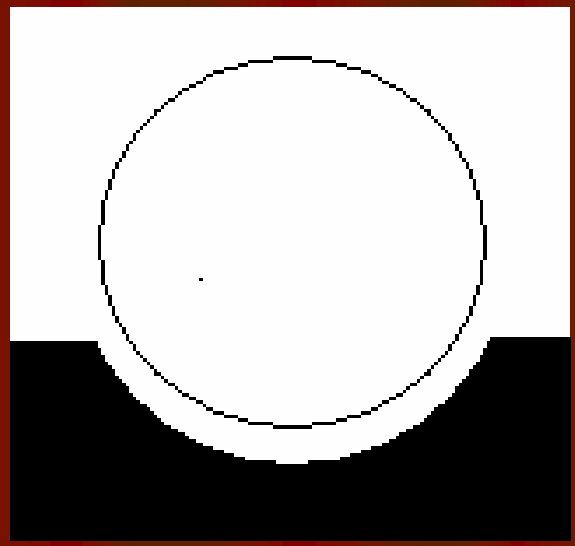

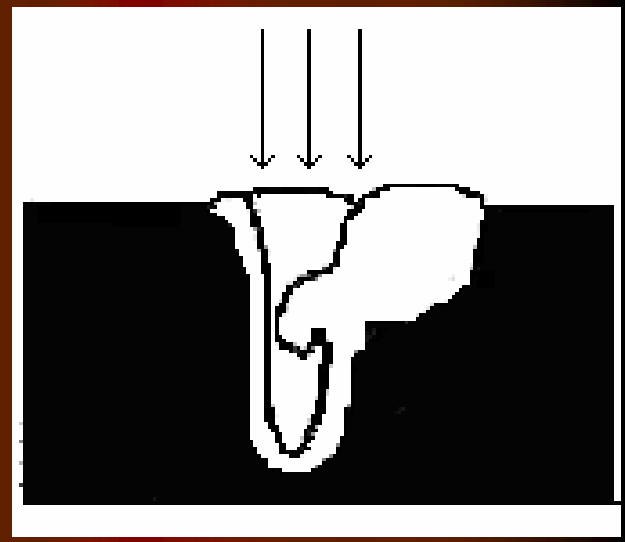

- Nucleation from super-saturation (Grigorenko,1970)
- Entrapment in high-intensity beam welding (Pastor et al. 2001)

Dept. Mechanical & Electro-Mechanical Eng., NSYSU
Kaohsiung, Taiwan, China

Nucleation (Ward et al. 1970; Wei et al. 2003)

Nucleation of a bubble on a surface is satisfied by

$$\frac{\partial \Delta F}{\partial R} \le 0, \qquad R \ge R_c$$

where the change in Helmholtz free energy

$$\Delta F = \sigma_{\ell g} A_{\ell g} + (\sigma_{sg} - \sigma_{s\ell}) A_{sg} - (p_g - p_\ell) V_g$$

where terms on the right-hand side are, respectively, free energy change due to formations of L-G and S-G interfaces and disappearance of S-L interface, and volumetric free energy change due to bubble formation

Continued

The free energy barrier for nucleation is

$$\Delta F_{max} = \frac{16\pi\sigma_{\ell g}^3}{3(p_g - p_\ell)^2} f(\phi) \qquad \text{where} \quad p_g = \eta p_{\ell,sat} + p_\ell \frac{C_{2,\ell}}{C_{2,\ell,sat}}$$

Factor $\eta \approx 1$, gas pressure is determined by considering phase equilibrium

$$\mu_{2,g}(p_g, T, \omega_{2,g}) = \mu_{2,\ell}(p_\ell, T, \omega_{2,\ell}) \qquad \mu_{1,g}(p_g, T, \omega_{1,g}) = \mu_{1,\ell}(p_\ell, T, \omega_{1,\ell})$$

The chemical potential for species j is evaluated by

$$\mu_j = \mu_{0j}(p, T) + k_B T \ln \omega_j$$

where $\mu_{0j}(p, T)$ is the chemical potential in the pure phase of species j, ω_j mole fraction.

$p_g = p_\ell = p_l \frac{C_{2,\ell}}{C_{2,\ell,sat}} + \eta p_{l,sat} = p_l$ (2)

Entrapment

- The reasons for entrapment of bubbles in liquid are still unclear. Bubble entrapment is closely related to complicated annular vertical two-phase flows.

Dept. Mechanical & Electro-Mechanical Eng., NSYSU
Kaohsiung, Taiwan, China

Model for Bubble Entrapment

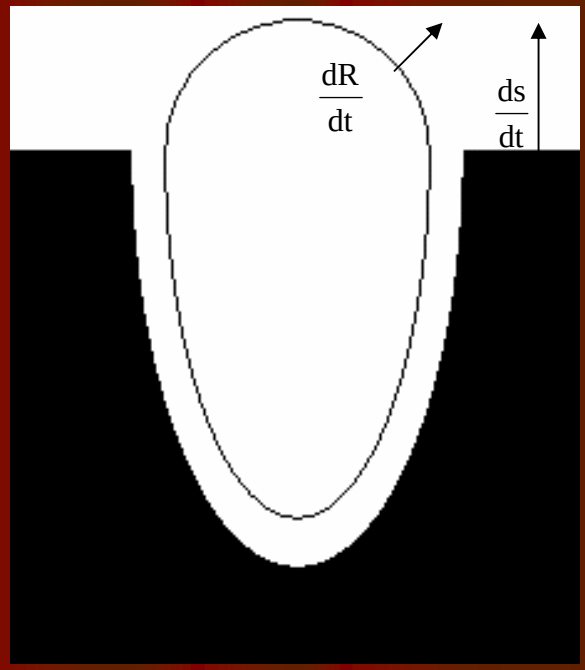

Previous two types of bubble formation can be treated by the model involving three phases separated by two moving boundaries

Dept. Mechanical & Electro-Mechanical Eng., NSYSU
Kaohsiung, Taiwan, China

Solution Procedure Chart

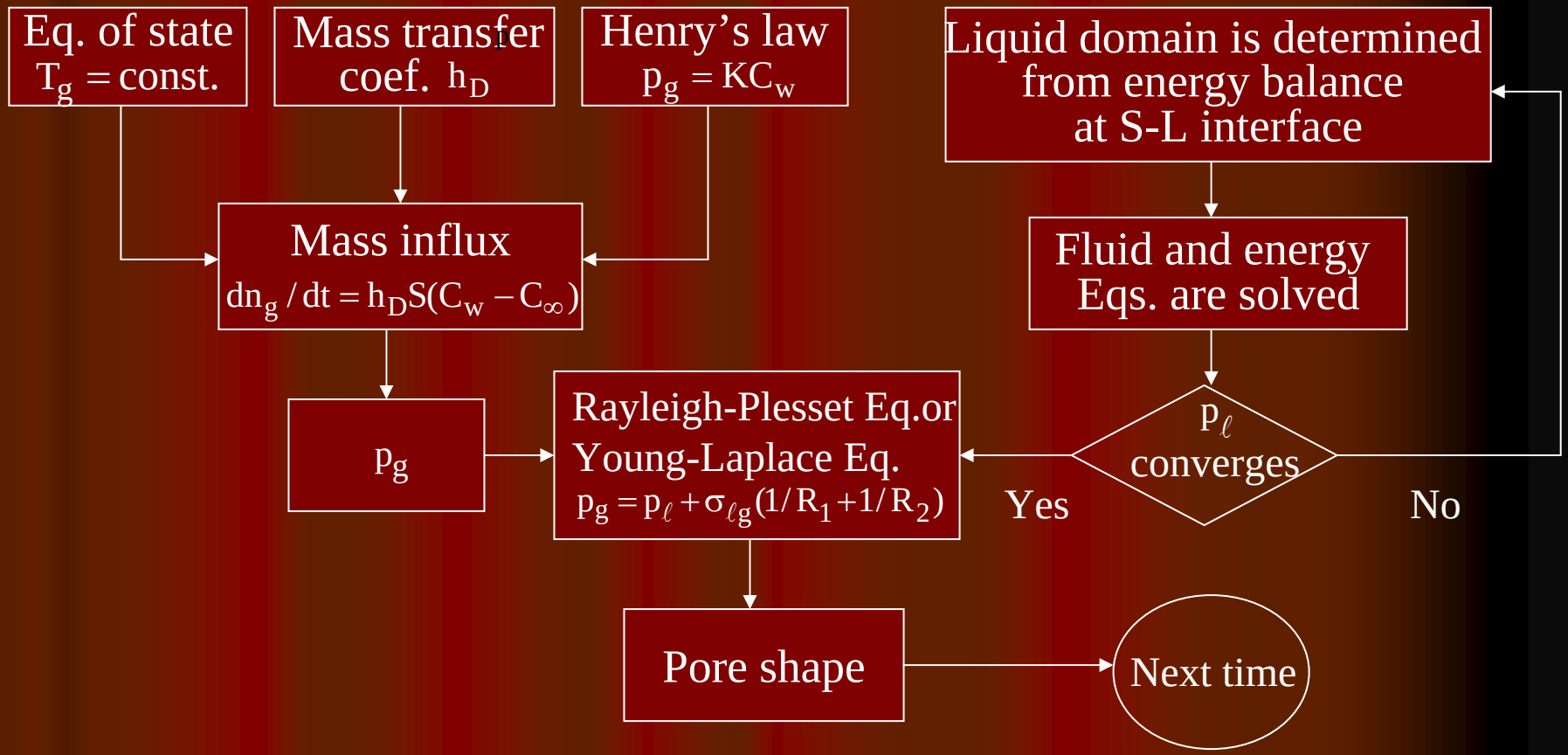

Dept. Mechanical & Electro-Mechanical Eng., NSYSU
Kaohsiung, Taiwan, China

Governing Equations and Boundary Conditions

Continuity, fluid, energy and species eqs.

$$\frac{\partial \rho}{\partial t} + \nabla \cdot \rho \vec{\mathbf{v}} = 0$$

$$\frac{\partial \rho \vec{\mathbf{v}}}{\partial t} + \nabla \cdot \rho \vec{\mathbf{v}} \vec{\mathbf{v}} = -\nabla p + \mu \nabla^2 \vec{\mathbf{v}} - \rho \beta_T \vec{g}(T - T_0) - \rho \beta_C \vec{g}(C - C_0)$$

$$\frac{\partial \rho T}{\partial t} + \nabla \cdot \rho \vec{\mathbf{v}} T = \alpha \nabla^2 T \qquad \frac{\partial \rho C}{\partial t} + \nabla \cdot \rho \vec{\mathbf{v}} C = D \nabla^2 C$$

Energy and concentration balances at the solidification front

$$-\vec{n} \cdot k_s \nabla T_s = -\vec{n} \cdot k_\ell \nabla T_\ell + \rho h_{s\ell} \vec{n} \cdot \vec{v} \quad \text{(i.e. Stefan B. C.)}$$

$$-\vec{n} \cdot D_s \nabla C_s = -\vec{n} \cdot D_\ell \nabla C_\ell + C_\ell (1 - k_p) \vec{n} \cdot \vec{v}$$

Simplified Models (Wei et al. 2000,2001,2004)

- Liquid pressure is hydrostatic pressure to avoid calculation of fluid equations.
- The bubble cap is spherical.
- The growth of bubble cap is specified.
- The liquid layer inside solid is stationary or absent.
- Henry's law is used to remove calculation of species transport.
- Solidification rate is a constant.

Dept. Mechanical & Electro-Mechanical Eng., NSYSU
Kaohsiung, Taiwan, China

Spherical Growth

- Schematic sketch gives

$$R + R\cos\phi \approx s$$

Differentiating leads to

$$\frac{dR}{dt}(1+\cos\phi) + R\frac{d\cos\phi}{dt} = \frac{ds}{dt}$$

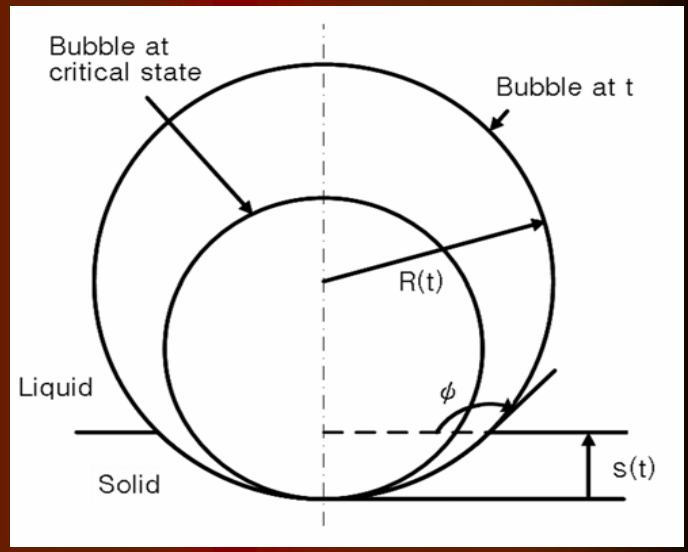

The contact angle is found by introducing $R = c\sqrt{t - t_N}$ and conducting integration

$$\phi = \cos^{-1}\left(\frac{\sqrt{t - t_N}}{c}\frac{ds}{dt} - 1\right) \quad \text{where} \quad c \equiv r_c\sqrt{\frac{3}{2\sigma}R_g T\omega M_{in,c}} \ .$$

Solidification Rate-Controlled Elongation

Normal stress balance gives

$$r_i(t) = \frac{2\sigma_{\ell g}\sin\phi}{p_g - p_\ell}$$

Concentration at the bubble cap can be simply obtained by

$$C_{\ell,w} = C_0\left(1 - \frac{K}{R_g T h_D}\frac{ds}{dt}\right)^{-1} \qquad (1)$$

which, unfortunately, exhibits singularity as denominator vanishes. Eq. (1) is derived as follow:

Continued

Differentiating Eq. of state

$$\frac{dp_g}{dt} V + p_g \frac{dV}{dt} = \frac{dn_g}{dt} RT \qquad (2)$$

where time derivative of bubble volume is

$$\frac{dV}{dt} = \pi r^2 \frac{ds}{dt} \qquad (3)$$

Mass inf lux is

$$\frac{dn_g}{dt} = h_D \pi r^2 (C_{\ell,w} - C_\infty) \qquad (4)$$

Henry's law is

$$p_g = K C_{\ell,w} \qquad (5)$$

Equation (1) is obtained from Eq.(2) by ignoring the first term and substituting Eqs. (3) through (5).

Dept. Mechanical & Electro-Mechanical Eng., NSYSU
Kaohsiung, Taiwan, China

Comparison between Prediction and Measurement

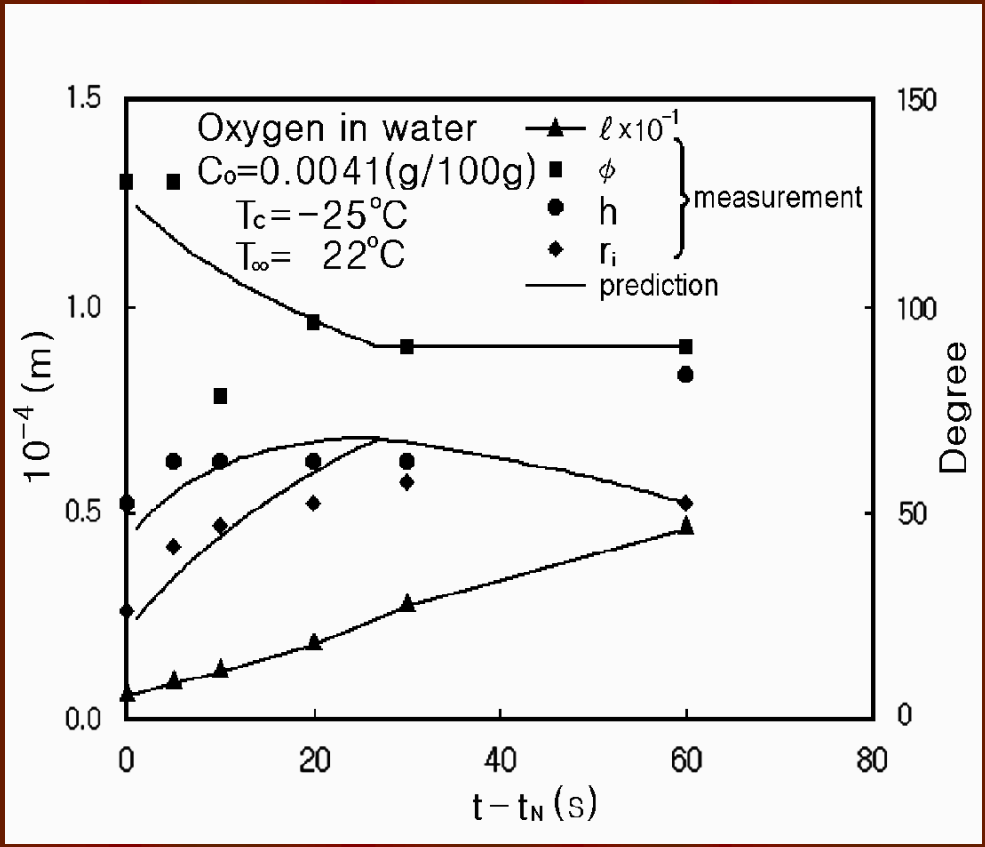

ℓ : bubble length in solid
ϕ : contact a ngle
h : cap height
r_i : cap radius on solidification front

Examples

- Example 1. Find (a) gas pressure, (b) free energy barrier for heterogeneous nucleation, and (c) the critical radius of a bubble in water containing oxygen gas of 0.0041 g/100g, as the solidification front advances to 1 cm. Solidification subject to a cold temperature of -25^{0}C starts at 20 cm below the free surface. The contact angle is assumed to be 60 deg.

Ans.: As shown in previous figure, oxygen content is 0.04 g/100g as the solidification front advances to 1 cm. The saturated solubility is 0.00665 g/100g, and saturation vapor pressure is 611 Pa.

(a) The difference in gas and hydrostatic pressures is

$$p_g - p_\ell = p_\ell\left(\frac{C_{2,\ell}}{C_{2,\ell,\text{sat}}} - 1\right) + p_{\ell,\text{sat}} = 1000 \bullet 9.8 \bullet (0.2 - 0.01) \bullet \left(\frac{0.04}{0.00665} - 1\right) + 611$$

$$= 9949 \text{ Pa}$$

(b) The free energy barrier is

$$\Delta F_{max} = \frac{16\pi\sigma_{\ell g}^3}{3(p_g - p_\ell)^2} f(\phi) = \frac{16\pi(0.076)^3}{3(9949)^2}(0.5 + 0.5^3)/4 = 1.2\times10^{-11}\,\mathrm{J}$$

(c) The critical radius is

$$R_c = \frac{2\sigma_{\ell g}}{p_g - p_\ell} = \frac{2\bullet 0.076}{9949} = 1.5\times10^{-5}\,\mathrm{m}$$

which agrees with experimental data (Wei et al. 2003)

- Example 2. As extended by Ex. 1, calculate (a) solidification rate, (a) mass transfer to the bubble at the time for nucleation.

  Ans.: (a) Energy balance at the solidification front is governed by

$$k_s \frac{\partial T_s}{\partial x} = k_\ell \frac{\partial T_\ell}{\partial x} + \rho h_{sl} \frac{ds}{dt}$$

Owing to low liquid thermal conductivity and thick thickness of liquid, solidification rate can be estimated by

$$\frac{ds}{dt} \approx \frac{k_s}{\rho h_{sl}} \frac{\partial T_s}{\partial x} \approx \frac{2.22}{1000 \bullet 3.3 \times 10^5} \frac{25}{0.01} = 1.7 \times 10^{-5}\, m/s$$

which agrees with experimental data.

Continued

(b) Choosing mass transfer coefficient h_D to be $1.7\times10^{-5}\,m/s$, mass transfer flux to the bubble yields

$$M_{in,c} = h_D(C_{\ell,w} - C_0) = 1.7\times10^{-5}(0.04-0.0041)\bullet\frac{10}{1000}\bullet1000$$

$$= 6.1\times10^{-6}\,kg/m^2-s$$

Example 3. Based on previous example, calculate the maximum radius of the pore as the solidification front is advanced to 3 cm.

Ans.: Henry's constant $K = 10^6$ Pa-m^3 / kg – mole, mass transfer coefficient $h_D = ds/dt = 1.7\times10^{-5}$ m / s. The solut content at the bubble cap is then calculated by

$$C_{\ell,w} = C_0\left(1-\frac{K}{R_g T h_D}\frac{ds}{dt}\right)^{-1} = 0.0041\left(1-\frac{10^6}{8314\cdot273\cdot1.7\times10^{-5}}1.7\times10^{-5}\right)^{-1} = 0.007 \text{ g/100g}$$

Gas pressure is

$$p_g = KC_{\ell,w} = 10^6\,\frac{\text{Pa}-\text{m}^3}{\text{kg}-\text{mole}}\cdot\left(\frac{0.007\text{g}/100\text{g}}{32}\cdot\frac{10}{1000}\right)\cdot1000\,\frac{\text{kg}}{\text{m}^3} = 2200 \text{ Pa}$$

The maximum radius takes place at a contact angle of $\pi/2$. This gives

$$r_i = \frac{2\sigma_{\ell g}}{p_g - p_\ell} = \frac{2\cdot0.076}{2200-1000\cdot9.8\cdot(0.2-0.03)} = 2.8\times10^{-4}\text{m}$$

which are of relevant magnitudes as experimental data.

Dept. Mechanical & Electro-Mechanical Eng., NSYSU
Kaohsiung, Taiwan, China

Wormhole Formation

$$(\text{Bond number} \equiv \frac{\rho g R^2}{\sigma_{\ell g}} \ll 1)$$

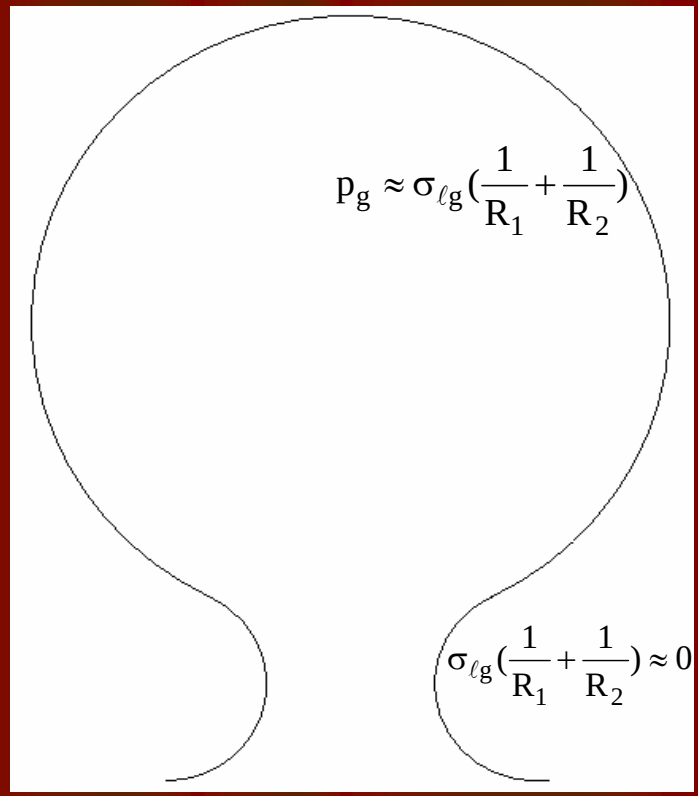

Balance between gas pressure and capillary pressure due to two principal curvatures results in a bubble having a neck.

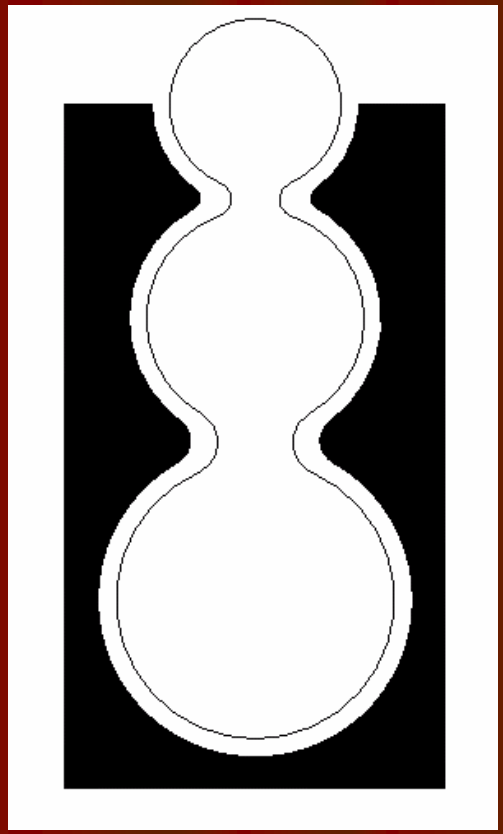

Force balance indicated in previous figure can be extended to interpret the formation of a wormhole. Furthermore, the reason for an increase in bubble size with depth is attributed to an increase in hydrostatic pressure

Future Topics

- Fluid flow effects on liquid pressure in bubble growth
- Gas flow in the bubble
- More realistic shape of the bubble surface
- Criterion for bubble departure and entrapment
- More realistic mass transfer across bubble surface
- Coupled solidification rate determined by energy equation together with Stefan boundary condition
- Interfacial morphology on bubble growth
- Interactions between adjacent bubbles and pores
- Cooling and solidification of a pore in solid
- Coalescence of pores in solid
- Criterions and phenomena among spherical, columnar, and periodic pores

Conclusions

- Mechanisms of pore formation in solid can be revealed from studying behavior of a bubble entrapped in solid during unidirectional solidification.
- Pore shapes in solid should account for transient phase changes in three phases, physico-chemical and metallurgical kinetics, mass, momentum, energy and species transport.
- Simplified models presented in this note have provided a fundamental and crucial understanding of pore formation in solid. However, they still need to be improved and generalized.
- Mechanisms of irregular shapes of pores are still unclear at the present time.

References

Dept. Mechanical & Electro-Mechanical Eng., NSYSU
Kaohsiung, Taiwan, China

- Chalmers, B., 1959, "How Water Freezes," Scientific American, Vol.200, pp.114-122.
- Geguzin, Ya. E., and Dzyuba, A. S., 1977,"Gas Evolution and the Formation and Capture of Gas Bubbles at the Crystallization Front When Growing Crystals from the Melt," Soviet Physics, Crystallography, Vol.22, pp.197-199.
- Geguzin, Ya. E., and Dzuba, A. S., 1981,"Crystallization of a Gas-Saturated Melt," Journal of Crystal Growth, Vol.52, pp.337-344.
- Grigorenko, G. M., 1970, "Formation of Pores in Welds," Avt. Svarka, No. 10, pp. 12-17.
- Pastor, M., Zhao, H., and DebRoy, T., 2001, “Pore Formation during Continuous Wave Nd:YAG Laser Welding of Aluminum for Automotive Applications,” Welding International, Vol. 15, pp. 275-281.
- Vasconcellos, K. F., and Beech, J., 1975,"The Development of Blowholes in the Ice/Water/Carbon Dioxide System," Journal of Crystal Growth, Vol.28, pp.85-92.
- Ward, C. A., Balakrishnan, A., and Hooper, F. C., 1970, "On the Thermodynamics of Nucleation in Weak Gas- Liquid Solutions," Transactions ASME Journal of Basic Engineering, Vol. 92, pp. 695-704

Continued

Dept. Mechanical & Electro-Mechanical Eng., NSYSU
Kaohsiung, Taiwan, China

- Wei, P. S. and Ho, C. Y.,2002, "An Analytical Self-Consistent Determination of a Bubble with a Deformed Cap Trapped in Solid during Solidification," Metallurgical and Materials Transactions B, Vol. 33B, pp. 91-100.
- Wei, P. S., Huang, C. C., and Lee, K. W.,2003,"Nucleation of Bubbles on a Solidification Front-Experiment and Analysis," Metallurgical and Materials Transactions B , Vol. 34B, pp. 321-332.
- Wei, P.S., Huang, C. C., Wang, Z. P., Chen, K. Y., and Lin, C. H., 2004,,"Growths of Bubble/Pore Sizes in Solid during Solidification -An In Situ Measurement and Analysis," Journal of Crystal Growth, Vol. 270, pp. 662-673.
- Wei, P. S., Kuo, Y. K., Chiu, S. H., and Ho, C. Y.,2000, "Shape of a Pore Trapped in Solid during Solidification." International Journal of Heat and Mass Transfer, Vol. 43, pp. 263-280.
- Wilcox, W. R., and Kuo, V. H. S., 1973,"Gas Bubble Nucleation during Crystallization," Journal of Crystal Growth, Vol.19, pp. 221-228.

Dept. Mechanical & Electro-Mechanical Eng., NSYSU
Kaohsiung, Taiwan, China

Thanks for Your Attention